

Aspects on high frequency power supplies for ESPs

Per Ranstad
Alstom Power
Sweden
per.ranstad@power.alstom.com

Jörgen Linner
Alstom Power
Sweden
jorgen.linner@power.alstom.com

1 Abstract:

High-frequency power supplies were originally introduced on the ESP market by ALSTOM (SIR) in 1993 [1, EPRI/DOE 1995]. An evaluation of the experiences gained during the first decade of operation was presented in [2, ICESP IX 2004]. It was found that the dust emissions were significantly reduced at the majority of the installations. Following the introduction of the first products, having a limited power capability, intense R&D efforts have been made in order to make this technology applicable to all sizes of ESPs. At higher power levels the efficiency and the operational temperatures are key design parameters.

It is the objective of this paper to present recent findings on the optimization of design and operation of high-frequency power supplies for electrostatic precipitators. Specifically, operational efficiency and availability will be discussed. Results from lab tests as well as operational data from the installed fleet (>2000 units) will be presented.

2 Introduction

High-frequency power supplies (HFPS) were originally introduced on the ESP market in 1993 [1]. An evaluation of the experiences gained during the first decade of operation was presented in [2]. Many publications have been made since the introduction of this technology, some examples are [3-5]. The aim of this paper is to discuss design aspects on power efficiency and availability.

A block diagram of high frequency power supply (HFPS) is presented in Fig. 1. The major difference compared to the mains frequency power supply is the much higher operational frequency, 25-50 kHz vs 50/60 Hz. The HFPS is fed from the three phase mains. The input voltage is rectified and supplied to a transistor-bridge configuration. The transistors are turned on and off in a sequence so that a high frequency voltage is applied to the transformer primary. The secondary of the transformer is rectified and connected to the ESP bus-section.

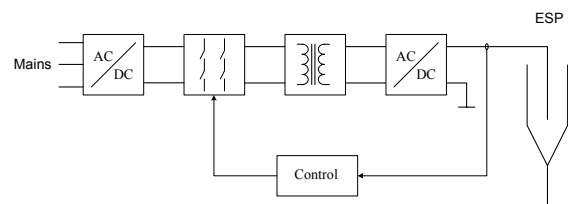


Fig. 1: Block diagram of a high frequency power supply, including the ESP bus-section

The most commonly used topology for HFPS on ESPs, the series loaded resonant (SLR) converter is shown in Fig. 2, [5]. It is estimated that more than 90 % of the installed fleet of HFPS is using this topology or derivatives thereof.

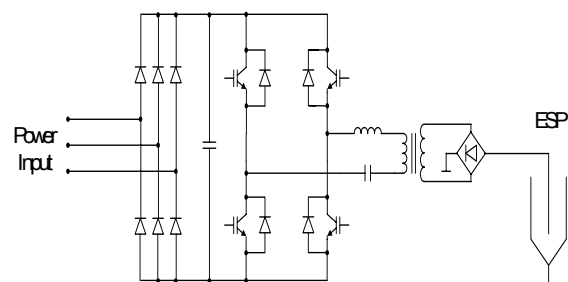


Fig. 2: Main circuit diagram, HFPS

The circuit contains a full bridge three-phase input rectifier followed by a DC-link capacitor. The DC-link voltage is converted into a high-

frequency voltage by means of an H-bridge (IGBT-inverter). The output of the H-bridge is connected to the primary of the high-frequency high-voltage transformer via a resonant tank. The purpose of the resonant tank is to control the switching losses by means of soft-switching. The transformer secondary is connected to a high-voltage rectifier which supplies the current to the ESP bus-section. Representing the HFPS by a current source, as shown in Fig. 3, indicates the pulsating output current, i_o , which is fed from the power supply to the load. In Fig. 3 a positive load current is indicated, this notation is used in the remaining part of the paper.

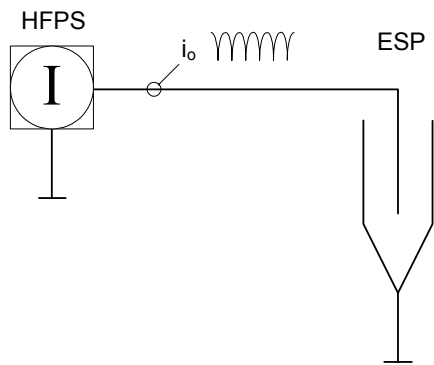


Fig. 3: Electrical system

The electrical characteristic of an ESP bus-section is given by the energy stored in the electrical field and the corona discharge. Fig. 4 indicates the corona discharge characteristic, i.e. the VI-curve [6]. From the diagram the non-linear characteristic is clearly indicated. Below a threshold voltage, U_{onset} , no corona discharge is present. However, above U_{onset} the current will increase with an increasing voltage, steeper at higher voltages. The operation is limited by the spark-over voltage, U_{spark} . In Fig. 4 an equivalent circuit of the bus-section is shown. The capacitance, C , represents the energy stored in the electrical field. The diode, D , and the non-linear resistance, R , represent the corona discharge characteristic.

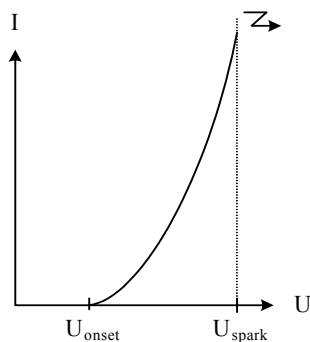


Fig. 4: Electrical characteristic, VI-curve

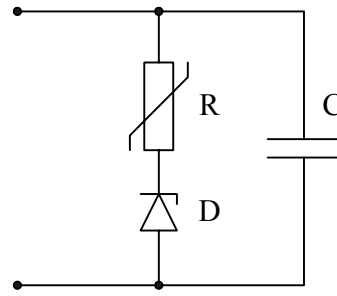


Fig. 5: ESP, equivalent circuit

Introducing the equivalent circuit of the ESP, Fig. 5, into the system of Fig. 3, results in the circuit shown in Fig. 6.

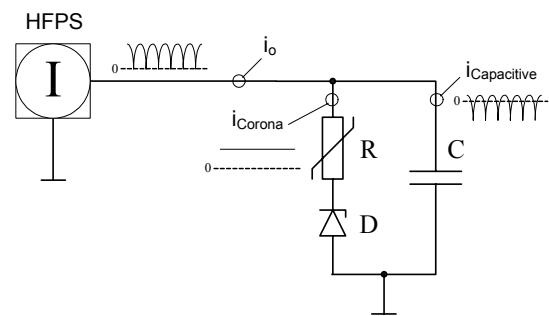


Fig. 6: Equivalent circuit

The capacitance of the buss section will act as a low impedance path for the high-frequency component of the current, thus filtering out almost any high-frequency component of the ESP voltage. The low-frequency component of the current (DC) is blocked by the capacitor and conducts through the corona discharge path (R, D). Hence, the ripple is very low when using HFPS. Applying typical values from ESP operation ($I=1 \text{ A}$, $U=50 \text{ kV}$, $C=100 \text{ nF}$, $f=30 \text{ kHz}$), yields a ripple voltage $< 0,16\%$.

3 Efficiency and thermal management

Efficiency is a key aspect of any power converter since the losses will generate heat and impact the power handling capability of the system. The local hot spots, in components and materials, are determined by the losses and the cooling system, i.e. thermal management. Moreover, for high power converter systems the losses may significantly impact the operational costs.

In this section different aspects on power conversion efficiency and thermal management are presented. IGBT losses as well as system aspects of the thermal management will be discussed. In section 2.1

are the frequency dependent conduction losses of IGBTs are presented. In section 2.2 'the influence of transformer parasitic components and their impact on the losses are discussed. Section 2.3 shows a method to improve the power capability of a converter system by means of modularization. For a more detailed analysis of the different aspects see, [5], [7-9].

3.1 Dynamic conduction losses

An evaluation of IGBTs is presented. The evaluation is made with respect to the on-state losses when conducting a high frequency sinusoidal current. It is expected that the time constant of the conductivity modulation make the losses to increase at higher frequencies.

The dynamic properties of the on-state voltage are studied under a sinusoidal current excitation. The current and voltage of the device under test (D.U.T.) are recorded. The instantaneous power loss is calculated as

$$p(t) = i(t) \cdot u(t) \quad (1)$$

The IGBT conduction losses, P , are calculated as the average of $p(t)$ as

$$P = \frac{2}{T} \int_0^{T/2} p(t) \cdot dt, \quad (2)$$

where T is the period time of the sinusoidal current.

P is calculated at varying temperatures and frequencies and is compared among the different test objects.

The test circuit as shown in Fig. 7 (a) consists of two half-bridges connected to a series resonant tank. The switches T_1/D_1 and T_2/D_2 are used to initiate an oscillation in the resonant tank. The switch T_4/D_4 serves as the D.U.T. and is continuously in the on-state. The on-state voltage U_{CE} and the conducted current I_E of T_4/D_4 is measured. The voltage E is adjusted such that the peak value of I_E , \hat{I}_E , is 150 A, which is kept constant for all measurements. The resonant tank components (L and C) determine the frequency.

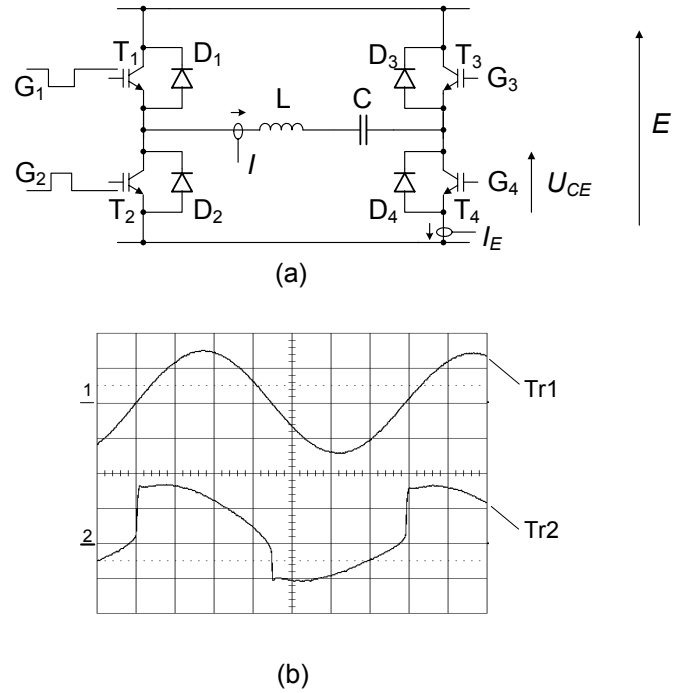


Fig. 7: Test system: (a) Circuit diagram, (b) Typical measurement, Tr1: I_E , Tr2: U_{CE} .

Fig. 7 (b) shows a typical oscillogram of the test circuit. The duration of the current oscillation is in the range of 1 ms and it is repeated at a low frequency, 0,5 Hz. The junction temperature, T_j , is controlled during the tests.

An important aspect of the measurements is the accuracy of $u_{CE}(t)$. At the actual frequencies the inductive voltage drop of the stray inductance of the module has to be compensated for.

Fig. 8 (a) and (b) show the on-state voltage at the different frequencies (including the DC equivalent), at 25 °C (a) and 125 °C, (b) for Device A. In order to compare U_{CE} at different frequencies the x-axis is scaled as the angle of the sinusoidal current. From the figures it can be observed that the on-state voltage is increased at higher frequencies. It is also observed that the higher temperature (125 °C) gives a higher on-state voltage, compared to the lower temperature (25 °C).

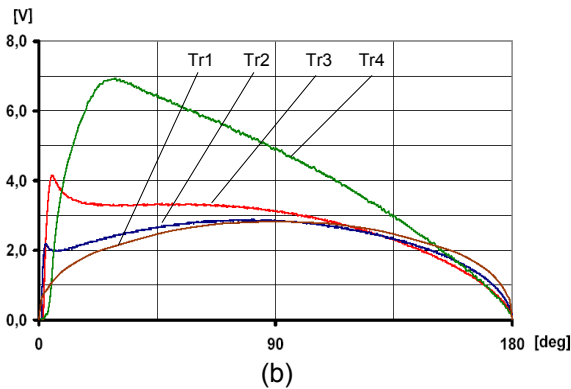
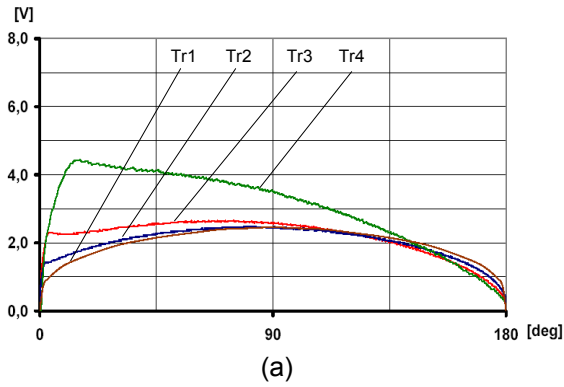


Fig. 8 Device A, U_{CE} , Tr1: DC eqv, Tr2: 7,5 kHz, Tr3: 30kHz, Tr4: 104 kHz:
(a) $T_j=25^\circ\text{C}$, (b) $T_j=125^\circ\text{C}$.

As an example, the lagging of the conductivity modulation is evident in Fig. 8(a) when comparing Tr1 (DC-eqv) and Tr2 (7,5 kHz). Before 90° (0- 90°). Tr2 shows a higher on-state voltage, while beyond 90° (90 - 180°) the on-state voltage is lower compared to Tr1. During the initial 90° the current is increasing, the time-constant of the conductivity modulation prevents the device to fully saturate. During the latter part of the conduction interval there is an excess of charges compared to the actual current, which results in a lower on-state voltage compared to the stationary case, Tr1 (DC-eqv).

From the analysis of Fig. 8 it appears that, for a rising current ($di_E(t)/dt > 0$), the time needed to fully develop the conductivity modulation causes an additional voltage drop. In a similar way, for a decreasing current ($di_E(t)/dt < 0$), the voltage drop is reduced due to the excess of charges. At the lower frequency, 7,5 kHz, these two effects are balancing and do not add significantly to the losses. However, at the highest frequency, 104 kHz, the increase of the on-state voltage during the first part of the sinusoidal current is heavily dominating over the decrease during the latter part. As a consequence, the power loss is significantly higher at the highest frequency.

Hence, the measurement proves the frequency dependency of the on-state losses, referred to as dynamic conduction losses. It is also evident that the operational temperature of the chip affects the frequency response.

The IGBT conduction losses, P , have been determined using (2). Fig. 9 shows the resulting losses for the different test devices as shown in Table 1. The losses are presented, for each device, at two different frequencies, 7,5 kHz and 30 kHz, and at two different temperatures, 25°C and 125°C .

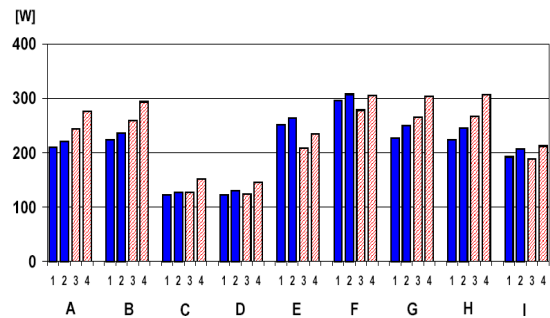


Fig. 9 IGBT conduction losses;
1: 7,5 kHz 25°C ,
2: 30 kHz 25°C ,
3: 7,5 kHz 125°C ,
4: 30 kHz 125°C

Table 1

Device	Denomination	Type
A	SKM400GB125D	NPT
B	FF300R12KS4	NPT
C	FF300R12KT4	PT
D	FF300R12KE4	PT
E	MG300Q2YS40	PT
F	CM300DY24NFH	PT
G	APTGF300A120	NPT
H	APTGF300A120*	NPT
I	CM300DC24NFM	PT

3.2 Comparison of LCC and SLR converters

In a real design of a high-voltage converter the parasitic elements of the transformer have to be considered. By the influence of the winding capacitance the SLR topology will convert into an LCC circuit, Fig. 10 [5,8]. The ratio $k = C_p/C_s$, is of importance for the

characteristics of the converter. For $k = 0$ the circuit turns into an SLR, while for $k = \infty$, the circuit becomes a Parallel Loaded Resonant converter, PLR. In the converters considered in this paper k is in the range of $0 < k < 0,25$. For these relatively low values of k , the SLR characteristics are dominant.

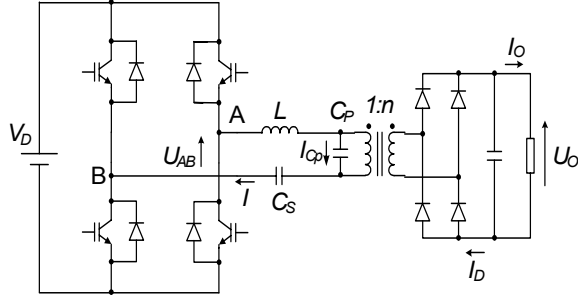


Fig. 10 LCC circuit diagram

The effect of C_P ($k = 0,25$) on the converter characteristics is indicated in Fig. 11. It is observed that the load lines are affected mostly in the upper part of the diagram, i.e. for high values of U_O . Consequently, the LCC converter will have the characteristics of a current source, which is beneficial for a voltage-stiff load such as an ESP.

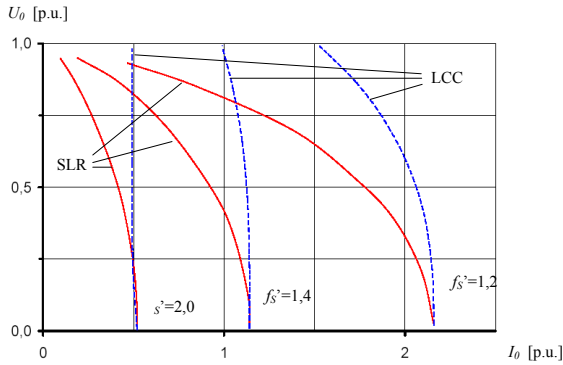


Fig. 11 Control characteristics for SLR (solid lines) and LCC ($k = 0,25$) (dashed lines)

Fig. 12 shows the effect of C_P in the time domain. At the zero-crossing of I the voltage of C_P has to reverse before the rectifier diodes can start to conduct. The associated charge Q_{C_P} is indicated in Fig. 12.

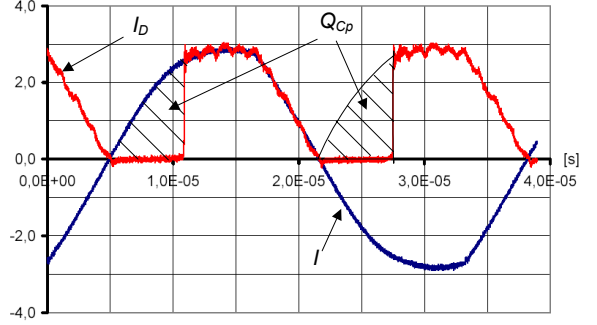


Fig. 12 Current waveforms showing the effect of C_P

During the discharging/charging of C_P the load is disconnected from the primary circuit. Q_{C_P} is determined by

$$Q_{C_P} = 2 \cdot C_P \cdot U_o' \quad (3)$$

where the reflected load voltage U_o' is given by

$$U_o' = \frac{U_o}{n} \quad (4)$$

In a power supply system the nominal output quantities U_{ON} and I_{ON} are determined by the operational area of the load. In an ESP application U_o and I_o need to be varied from zero to the nominal values independently, determined by the actual dust-load conditions. By properly choosing the transformer turns ratio, n , the operating area referred to the primary side of the transformer may be optimized. The conversion ratio, d is defined as

$$d = \frac{U_o'}{V_D}, \quad 0 < d < 1. \quad (5)$$

The highest value of $d = d_{MAX}$ is obtained at $U_o = U_{ON}$. Hence, U_{ON} and I_{ON} reflected to the primary can be written as

$$U_{ON}' = d_{MAX} \cdot V_D \quad (6)$$

$$I_{ON}' = \frac{I_{ON} \cdot U_{ON}}{d_{MAX} \cdot V_D} \quad (7)$$

From (7) it is found that it is beneficial to choose a high value of d , since this lowers the IGBT current and consequently the losses are reduced. However, in a frequency controlled SLR, a high value of d requires the system to operate close to the resonance frequency, $f_s' \approx 1$ (as indicated in Fig. 11.) which may give rise to difficulties in the control of the

converter. Typically, in an SLR the value of d_{MAX} is chosen in the range of 0,7-0,8. Considering an LCC topology, which shows current-source characteristics, f_s' is not affected in a similar way, as shown in Fig. 11. Consequently, d may be given a comparably higher value in an LCC than in an SLR. As indicated in [8] in the case of an LCC d is limited by the operation of the capacitive snubbers.

Loss reductions as a result of the higher d of the LCC converter are shown experimentally on a 40 kW / 25 kHz converter ($k = 0,15$) [8]. Table 2 gives the resulting IGBT losses at different values of d_{MAX} . In the experiments #1 and #4 C_p is disconnected ($k = 0$).

Table 2

	d_{MAX}	P [W]	I_o	U_o
#1	0,76	934	I_{ON}	$0,1 U_{ON}$
#2	0,89	708	I_{ON}	$0,1 U_{ON}$
#3	1,01	606	I_{ON}	$0,1 U_{ON}$
#4	0,76	795	I_{ON}	U_{ON}
#5	0,89	696	I_{ON}	U_{ON}

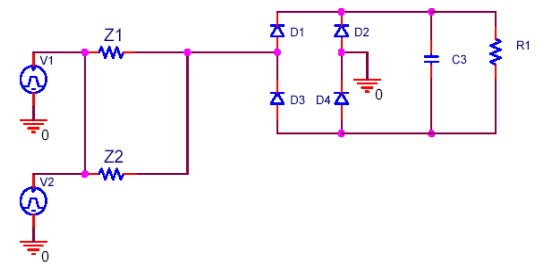
3.3 Loss handling by means of modularization

The main circuit of an SLR designed for three-phase off-line operation can be divided into different subsystems: input rectifier, IGBT-bridge, resonant tank, transformer, and output rectifier, Fig. 4. The IGBT-bridge is the main contributor the loss budget, typically generating 50-60% of the total losses. In order to distribute the losses and thereby increase the power handling capability of the system modularization may be utilized [9].

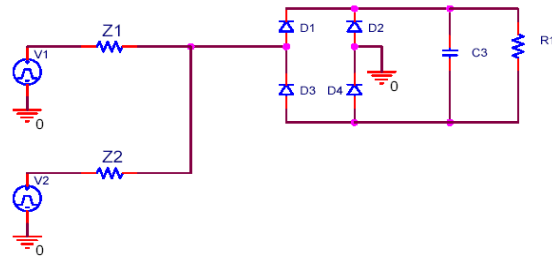
An even load distribution among the modules is a key issue in a modularized system. Furthermore, the load sharing shall be robust with respect to operating frequency, variation in components and parasitic elements.

Fig. 12 shows three different ways of modularizing the SLR. The sources V1 and V2 represent two paralleled modules each comprising input rectifier and IGBT bridge. The analysis assumes the IGBT-bridges to be operated in phase and having the same voltage amplitude. The first alternative, as shown in Fig. 12(a), is formed by simply paralleling the IGBT-bridges. This method suffers from a poor load sharing. The current in a branch is determined by parasitic parameters of the

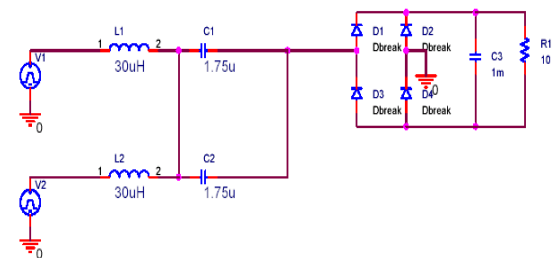
semiconductors and of the main circuit layout. Fig. 12(b) shows the paralleling of the IGBT-bridges with separate resonant tanks. The currents are summed at the primary of the transformer. The load sharing is determined by the ratio of the impedances Z1 and Z2. This ratio is very sensitive to parameter variations in C and L, specifically when operated close the resonance. In the proposed method, as shown in Fig. 12(c) a connection is added between the midpoints of the tanks. This method controls the load sharing by the ratio of the parameter values of the inductors, L1 and L2. The ratio is stable over a wide frequency range and robust to parameter variations of the inductors and the IGBTs.



(a)



(b)



(c)

Fig 12 Cascading : (a) at bridge output, (b) at transformer primary , (c) proposed method.

In order to evaluate the proposed method, as shown in Fig. 12(c), an experimental system was designed comprising two IGBT-bridges and a common transformer/output rectifier. The system ratings are; 120 kW/70 kV. The system is fed from an industrial grid, 3*500VAC. Fig. 13 shows the circuit diagram of the experimental system. From the measurements

presented in Fig. 14 an even load sharing is evident.

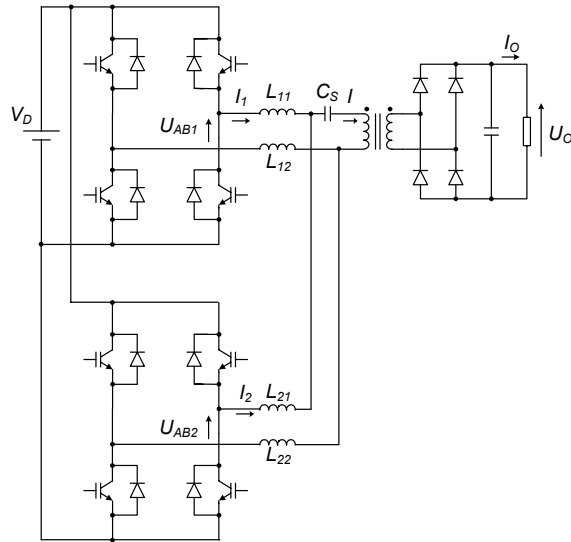


Fig. 13 Experimental set-up, circuit diagram.

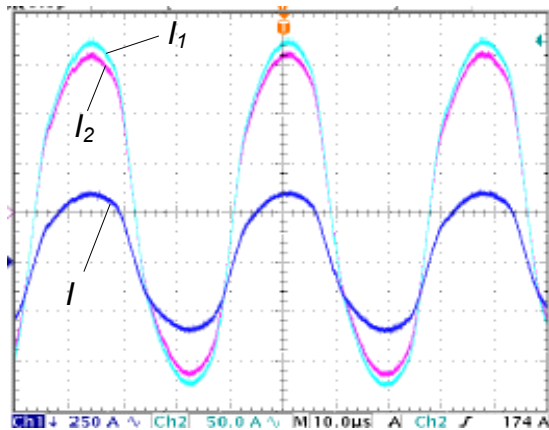


Fig. 14 Experimental result: I_1 (50A/div), I_2 (50A/div), I (250A/div, offset -250A).

4 Availability

The availability of ESPs operating in power plants or in industrial processes is of great importance. If the full functionality of the ESP is not available, when required, the production of the main process (power generation or industrial process) has to be reduced.

The availability of a system is given by its failure rate and time to repair (down time). The failure rate is often given by its inverse, Mean Time Between Failures (MTBF). The down time of a properly designed HFPS is 1-2 hours. This is

due to the integrated design and predefined spare parts.

The reliability of HFPS has been an issue during the introduction period of this technology. However, in [2] a measured MTBF value of 17 yrs was presented from a fleet of 820 HFPS during 3 months of operation. It was also concluded that the reliability of HFPS would increase furthermore due to feedbacks from field operations to product improvements.

In 2008 Alstom introduced a new high-voltage unit design (transformer and output rectifier). At the time of the writing of this paper (2011/04) 368 of these have been installed, the estimated time of operation is 533 yrs. Out of this fleet the MTBF is found to be higher than 200 yrs.

5 Conclusion

A general analysis of the operation of HFPS in continuous mode including an electrical model of the ESP has been presented. The voltage ripple originating from the high-frequency current component has been estimated and found to be very low, $< 0,2\%$.

Three different aspects on efficiency and thermal management are presented. The dynamic conduction losses are analyzed and experimental results are presented for nine commercially available IGBT modules. The result shows that equally specified components may behave differently in this respect. It is shown how the parasitic capacitance of the high-voltage transformer can be utilized in the circuit to obtain lower losses in the IGBTs. This is due to that a higher conversion ratio can be used in an LCC operated above the resonance. By the use of a modularization of the dominant loss source (IGBT bridge) the operational temperatures of the components can be reduced and consequently the reliability is improved.

The availability of high frequency power supplies for ESPs are discussed. Results of reliability measurements on a new transformer design shows a mean time between failures exceeding 200 yrs.

6 Literature

- [1] P. Ranstad and K. Porle, "High frequency power conversion: A new technique for ESP energization", Proceedings of the EPRI/DOE International Conference on Managing Hazardous and Particulate Air Pollutants, Toronto, Canada, August 1995.
- [2] P. Ranstad, C. Mauritzson, M. Kirsten, R. Ridgeway, "On experiences of the application of high-frequency power converters for ESP energisation, " Proceedings of the 9th International Conference on Electrostatic Precipitation, ICESP IX, Mpumalanga, South Africa, May 2004.
- [3] N., Grass, W., Hartmann, M., Klöckner; "Application of different Types of High Voltage Supplies on Industrial Electrostatic Precipitators"; IEEE Transactions on Industry Applications, vol. 40, No. 6, Nov./Dec.; 2004
- [4] R., Seitz, H., Herder; "Switch Mode Power Supplies for Electrostatic Precipitators"; Proceedings of the 8th International Conference on Electrostatic Precipitation, ICESP VIII, Birmingham, Al, USA, May 2001.
- [5] P. Ranstad, "Design and Control Aspects on Components and Systems in High-Voltage Converters for Industrial Applications, " PhD Thesis, Royal Institute of technology, Stockholm, Sweden, Oct 2010.
- [6] K. R., Parker; "Applied electrostatic precipitation"; Blackie Academic & Professional; ISBN 0 7514 0266 4; 1997
- [7] Ranstad, P., Nee, H-P, "On dynamic effects influencing IGBT losses in soft switching converters", IEEE Transactions on Power Electronics, vol. 26, No. 1, Jan., 2011
- [8] Ranstad, P., Demetriades G. D., "On conversion losses in SLR and LCC-topologies", The 3rd Mediterrean Conference and Exhibition on Power Generation, Transmission and Energy Conversion, MEDPOWER 2002, Athens, Greece, November 2002
- [9] Ranstad, P., Demetriades, G.D., Nee, H.-P.; "On cascading of the SLR", Proceedings of the 39th IEEE Power Electronics Specialists Conference, PESC '08, Rhodes, Greece, June 2008